Editors
Robert A. Scott · Charles M. Lukehart

Applications of Physical Methods
to Inorganic and Bioinorganic Chemistry

WILEY

Visit the online Encyclopedia of Inorganic Chemistry at
www.mrw.interscience.wiley.com/EIC/

EIC Books

High Resolution Electron Energy-Loss Spectroscopy

Manuel P. Soriaga, Xiaole Chen and Ding Li

Texas A&M University, College Station, TX, USA

John L. Stickney

University of Georgia, Athens, GA, USA

METHOD SUMMARY

Acronyms, Synonyms
- <u>H</u>igh-<u>r</u>esolution <u>E</u>lectron <u>E</u>nergy-<u>L</u>oss <u>S</u>pectroscopy
- <u>E</u>lectron <u>E</u>nergy-<u>L</u>oss <u>S</u>pectroscopy.

Measured physical quantities
- the number of counts (intensity) as a function of the energy loss of inelastically backscattered low-energy electrons.

Information available
- the vibrational modes, and the corresponding energies, of species at the interface: substrate, physisorbed adsorbate, chemisorbed adsorbate, adsorbate–adsorbate interactions.

Information not available, limitations
- The properties are not related to the vibrational modes of the interfacial species.

Examples of questions that can be answered
- What molecular species are present on the surface?
- What is the mode of bonding between the adsorbate and the substrate?
- How does the surface chemical bond influence the vibrational properties of the adsorbate?
- What is the surface coverage of the adsorbed species?

Major advantages
- extremely sensitive; limit of detection is ca .0.01% of a monolayer
- broad spectral range; typically, 50 (6.2 meV) to 4000 cm^{-1} (496 meV)

- impact-scattering mechanism not restricted by selection rules; in combination with dipole scattering, all vibrational modes may be discernible
- nondestructive.

Major disadvantages
- an ex situ method requiring an ultrahigh vacuum environment
- comparatively low resolution: typically, $30\,cm^{-1}$ ($3.7\,meV$); at best, $4\,cm^{-1}$ ($0.5\,meV$)
- backscattering may be inhibited by cationic species.

Sample constraints
- The sample surface must be conductive and relatively smooth.

1 INTRODUCTION

A vast amount is now known, at the atomic level, about heterogeneous processes at gas–solid interfaces. Yet, three decades ago, research in solid surface science was mired in traditional thermodynamic and kinetic experiments that were not able to yield molecular level information. Fundamental issues, such as the molecular structure and chemical composition of the surface complex, could not be adequately addressed by the data generated from the classical methods. It was not until the development of highly surface-specific empirical tools that tangible gains in the study of the gas–solid interface were achieved.

The main difficulty in surface characterization lies in the exceedingly low population of surface atoms (10^{15} atoms cm^{-2}) relative to that of bulk species (10^{23} atoms cm^{-3}). Experiments intended to examine the physical and chemical properties of surfaces must employ techniques that interact only with the outermost layers. For example, standard structural tools such as (nongrazing incidence) X-ray diffraction are not applicable to single-crystal surfaces since X rays penetrate deeply into the material and yield information on the bulk rather than the surface.

The majority of interfacial characterization techniques take advantage of the unique surface sensitivity of low-energy electrons. Such surface specificity arises because the mean free path of an electron through a solid is dependent upon its kinetic energy.[1,2] In particular, an electron whose kinetic energy is between 10 and 500 eV can traverse no more than 2 nm within the solid. Hence, the ''interrogation'' of low-energy electrons emergent from a sample will bear information that is specific only to the surface.

A solid subjected to a beam of electrons of primary (incident) energy E_p gives rise to backscattered (primary) and emitted (secondary) electrons. The energy distribution of these electrons can be divided into four regions based upon the origin of the scattered electrons. These regions correspond to the following: (i) True secondary electrons, are created from multiple inelastic interactions between the incident and bound electrons; these electrons give rise to an intense broad band at the lower end of the spectrum. (ii) Auger electrons which, along with primary electrons inelastically scattered by surface electronic states, are responsible for the small peaks in the medium-energy range. (iii) Primary electrons, which are inelastically scattered upon interactions with surface vibrational states; peaks associated with these electrons reside close to the elastic peak as their energy losses are comparatively small. (iv) Primary electrons, which are scattered elastically; such electrons, comprise only a small percent of the total incident electrons, and they generate the elastic peak at E_p. Regions (ii) to (iv) of the energy spectrum have been exploited in modern surface-structural and interfacial-elemental analysis. The elastic peak, for example, is used in diffraction experiments. The peaks in Region (iii) form the basis of high-resolution electron energy-loss spectroscopy (HREELS).

2 TECHNICAL BACKGROUND

2.1 Energy-Loss Mechanisms

Almost all of the electrons incident at a solid surface undergo inelastic events that cause them to be backscattered at energies lower than their initial or primary energy E_p. If E_l is the energy lost to the surface, peaks would appear in the spectrum at energies $\Delta E = E_p - E_l$. Such peaks, commonly referred to as energy-loss peaks, originate from core-level ionizations, valence-level excitations, plasmon losses, or vibrational excitations.[1,2] Since $E_{vibrational} < 4000\,cm^{-1}$ ($0.50\,eV$)[a], the vibrational energy-loss peaks lie close to the elastic peak and can be observed only if electron-energy discrimination is carried out at high resolution.

Two mechanisms give rise to high-resolution electron energy-loss (HREEL) spectra[1–8]: dipole scattering and impact scattering. In dipole scattering, the incident electron may be treated similarly to an electromagnetic (infrared) wave that interacts, at long range, with oscillating dipoles created by the vibration of species at the surface. Dipole-scattering HREELS is thus governed by the well-known harmonic-oscillator[b]

infrared selection rules: At ambient temperatures, (i) only fundamental transitions are allowed; and (ii) only vibrations accompanied by a change in dipole moment are observed.

On metal surfaces, two additional selection rules apply. The first is that only vibrations perpendicular to the surface are HREELS active. This rule follows from two phenomena unique at metal surfaces[3–8]: (i) Electromagnetic waves polarized perpendicularly to the plane of incidence (parallel to the plane of the surface) undergo a 180° phase shift upon reflection. That is, at the metal surface, the out-of-phase electric-field vectors of the incident and reflected waves cancel each other; as a result, no field exists that can couple with dipoles that oscillate parallel to the surface. (ii) The dynamic dipole moment generated by an oscillator that vibrates in the surface-parallel direction is cancelled by that of its image dipole (Figure 1); hence, there the net dynamic dipole moment is zero. On the other hand, if the real dipole is oriented perpendicularly to the surface, its dynamic dipole moment is reinforced by that of its image dipole. This selection rule is the same as that for infrared reflection-absorption spectroscopy (IRAS).[c]

The second dipole-scattering selection rule states that the intensity is at a maximum when the angle of collection is the same as the angle of (specular) reflection. This selection rule is illustrated in Figure 2; the intensity of the dipole-scattered peak at 130 meV (1050 cm^{-1}) falls precipitously as soon as the collection angle deviates from the specular angle. Figure 2 also shows that the angular dependence of the elastic peak is the same as that of the dipole-scattered peak.

The mechanism for impact scattering at solids is rather complex as it involves the penetration of the incident electron into the adsorbed molecule; the theoretical treatment requires a quantum mechanical formalism. The transfer of energy from the incident electron to a vibrational mode occurs, within a very short time, while the electron is inside the molecule. The dipole-scattering selection rules do not apply to impact scattering. Theoretical considerations have predicted, and experimental studies have confirmed, the following "propensity rules" for this mechanism[4]: (i) Impact scattering
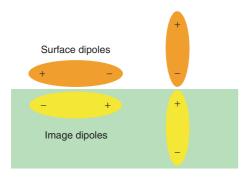

Figure 1 The dynamic electric moment of the dipole oriented parallel to the metal surface is cancelled by that of its image dipole. In the vertical orientation, the dynamic electric moments of the surface and image dipoles reinforce each other
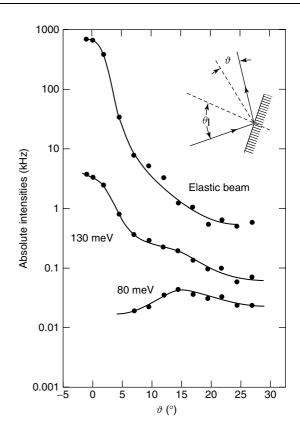

Figure 2 The influence of off-specular angle (φ) on the absolute peak intensities in dipole scattering (130 meV) and in impact scattering (80 meV). (Published in Electron Energy Loss Spectroscopy and Surface Vibrations, Ibach H & Mills D L, © Elsevier 1982)

vanishes in the specular direction; that is, impact-scattered peaks can be observed only if detection is at angles removed from the specular direction. The dependence of impact scattering on the off-specular scattering angle (φ), where φ is the deviation of the collection angle from the angle of (specular) reflection, is shown in Figure 2.[4] Impact scattering (80 meV (645 cm^{-1})) is most prominent when $\varphi \sim 15°$. (ii) Impact scattering is more likely to be dominant, even at low off-specular angles, at higher vibrational energies. (iii) Strong dipole scatterers are weak impact scatterers; conversely, weak dipole scatterers are strong impact scatterers.[d]

It is clear that the combination of specular and off-specular HREELS provides a means for the complete identification of the normal modes of an adsorbed molecule; considerations based upon point-group and space-group theory would, of course, be required. HREELS is an extremely sensitive technique. The limit of detection for strong dipole scatterers such as CO can be as low as 0.0001 monolayer; for weak scatterers such as hydrogen, the limit is 0.01 monolayer. In comparison, IRAS for chemisorbed CO, a strong infrared absorber, is restricted to coverages above 0.1 monolayer. HREELS studies of non-CO organic molecules adsorbed at atomically smooth surfaces are abundant; similar experiments using IRAS are meager. The energy accessible to HREELS

ranges from 50 (6.2 meV) to 4000 cm^{-1} (496 meV); common IRAS detectors are not useful below 600 cm^{-1} (74 meV). On the other hand, IRAS has higher-resolution (nominally 4 cm^{-1}) than HREELS (typically 30 cm^{-1} (3.7 meV)), although resolutions of up to 4 cm^{-1} (0.25 meV) have been claimed for the latest models of (Ultrahigh-resolution electron energy-loss spectroscopy (UHREELS)) instruments.[7] The primary limitation of HREELS is that the apparatus is quite specialized, rather delicate and requires an ultrahigh vacuum (UHV) environment; IRAS can be carried out under ambient conditions. It has recently been observed that countercations present in the adsorbed layer may block low-energy electron backscattering.[8]

2.2 Instrumentation

Figure 3(a) shows a schematic diagram of a first-generation HREEL spectrometer.[3] In this model, the energy of incident electrons can be varied from 1 to 10 eV. To afford high-resolution, energy monochromation and analysis are done either with a cylindrical mirror analyzer, cylindrical deflector, or spherical deflector analyzers in combination with retarding-field optics. Off-specular collection of the backscattered electrons is afforded by rotation of either the sample or the analyzer. Owing to extremely low signals (10^{-10} A), continuous dynode electron multiplier detectors are employed. Figure 3(b) is a photograph of an UHREELS spectrometer.[7] This model consists of an electron gun, a two-stage monochromator, a single-stage energy analyzer, and a channel electron multiplier detector. Both energy monochromation and energy analysis are carried out with 127° cylindrical deflection analyzers. The incident electrons have an initial energy spread of 0.3 eV. The two-stage monochromator serves to narrow the energy spread to <1 meV and generate a highly monoenergetic beam of low-energy electrons (typically 1 to 10 eV). A zoom lens system focuses and accelerates the electron beam onto the sample. The backscattered electrons are passed through a separate zoom lens for focusing and deceleration before they are sorted out by a single-stage energy analyzer into the detector. The signal is fed to a preamplifier as pulses for electron counting. The analyzer is designed to be rotatable from 0° to 78° for off-specular (impact-scattering) measurements.
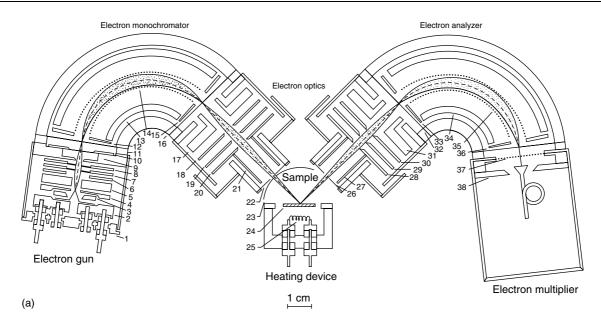
3 SELECTED APPLICATIONS
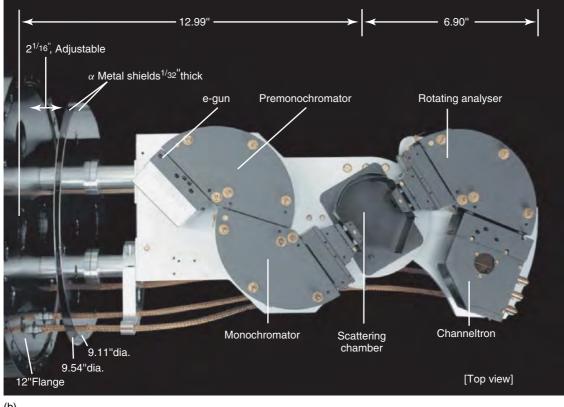
3.1 Inorganic Molecules

3.1.1 Carbon Monoxide

Carbon monoxide is the most widely used molecular probe in the study of the coordination chemistry and catalytic reactivity of metal surfaces. The chemisorption of CO at transition-metal surfaces is similar to the coordinate-covalent bond formation in homogeneous metal–carbonyl complexes.[9–11] The interaction initially involves a σ bond formed by the electron-pair donation from a filled spσ ligand orbital to an unoccupied dσ metal orbital; this is followed by a π bond created by the electron-pair back-donation from a filled dπ (or dpπ) metal orbital to an empty $2\pi^*$ ligand orbital.[9,10] As a result of the surface coordination, the C≡O bond is weakened and ν_{CO}, the vibrational frequency of the C≡O stretch mode (2142 cm^{-1} (266 meV) in the gas phase) undergoes an appreciable redshift. The larger the extent of the back-donation, the stronger the metal–carbon (M–C) interaction, and the weaker the C≡O bond. The degree of π back-donation is also heightened by an increase in the number of surface atoms bridged by the CO ligand. In the latter case, multiple M–C bonds will be expected; for example, CO chemisorbed on a threefold hollow site will most likely be bonded to three different metal atoms. Consequently, ν_{CO} will display strong dependence on site geometry[11]: At ''atop'' (onefold) sites, ν_{CO} lies in the range from 2000 (248 meV) to 2130 cm^{-1} (264 meV); at twofold bridge sites, ν_{CO} falls between 1840 (228 meV) and 1960 cm^{-1} (242 meV); and for threefold bridge sites, ν_{CO} appears in the range from 1800 (223 meV) to 1920 cm^{-1} (238 meV). HREELS has been employed in the study of CO chemisorption on most transition metals.[12–26] Bimetallic[22] and oxide surfaces[23,24] relevant in catalytic oxidation have also been investigated.

Since the infrared absorptivity of the C≡O stretch mode is fairly large, IRAS has also enjoyed widespread use in the study of CO chemisorption. However, for the investigation of the metal–carbon vibrational mode, IRAS may not be the technique of choice since the frequency of this mode (ν_{M-CO}) lies below 400 cm^{-1} (50 meV), a region in which nonsynchrotron-based sources are quite weak and wide-range photoconductive detectors suffer degraded sensitivity. Studies on the metal–carbon stretch mode may be more reliably investigated by HREELS, although (infrared) sum-frequency generation also seems viable.[27] The expectation is that, since ν_{CO} is dependent upon adsorption-site geometry, ν_{M-CO} will likewise be influenced by it. For example, on Rh(111), it has been found that ν_{M-CO} was highest when the ligand was coordinated on a onefold site and lowest when located on a threefold site.[28] This observation may appear inconsistent with the fact that linearly bonded CO has the weakest metal–carbon bond. But it must be noted that an atop site attached CO has only one M–C bond, whereas a threefold-site-bonded CO would have three distinct bonds with three different metal atoms. While the combined strength of the three bonds would be greater than just one bond, the vibrational energy of each of the three (degenerate) bonds would, individually, not be as high. Of course, the role of dipole–dipole interactions in the observed frequency shift cannot be discounted since the shifts become pronounced at near-monolayer coverages where lateral interactions become significant.[28]

(a)

1 cm

(b)

Figure 3 (a) Schematic diagram of first-generation HREEL spectrometer. (Reprinted from Froitzheim.[3] With kind permission of Springer Science & Business Media); (b) Photograph of a modern ultrahigh-resolution EEL spectrometer. (Reprinted from http://www.lktech.com/products/els5000.html, courtesy of LK Technologies, Inc)

Two other HREELS studies of dipole–dipole coupling will be mentioned. One focused on Ni(100) and involved the determination of the effect of temperature and coverage on ν_{CO}.[13] The results are displayed in Figure 4. The

peak near 50 meV (400 cm^{-1}) was associated with ν_{M-CO} and the peaks at 240 (1920 cm^{-1}) and 250 meV (2016 cm^{-1}) were assigned, respectively, to ν_{CO} at twofold and atop sites. At 150 K, only one peak, due to bridge-bonded CO, was observed
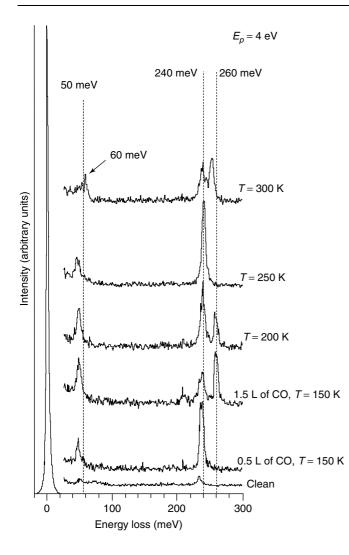
Figure 4 HREEL spectra of CO on Ni(100) for 0.5 L and 1.5 L of CO and thermal behavior of the 1.5 L CO in the 150–300 K range. (Reprinted from Formoso, Marino, Chiarello, Agostino, Caruso and Colavita,[13] © Elsevier 2006)

at submonolayer coverages. At near-monolayer coverage, a second prominent peak emerged at 260 meV (2097 cm^{-1}). The latter was not assigned to atop site-bonded CO since ν_{CO} for that is only 250 meV. A dipole–dipole interaction between adjacent CO molecules was thus postulated. It was thought that this type of coupling would weaken the metal–CO bond because of reduced π-back donation; the latter, in turn, would strengthen the C≡O bond and lead to the blueshift of ν_{CO}. Further evidence for the dipolar interactions was provided by the decrease in the intensity of the 260-meV peak as the temperature is raised; an increase in temperature tends to disrupt dipole–dipole coupling. At 300 K, CO coordinated at twofold and atop sites, devoid of dipole–dipole interactions, were indicated.

The other study examined the influence of Sn adatoms on the dipole–dipole interactions at Pt single-crystal surfaces.[22] On Pt(110), CO was bonded predominantly on

atop sites at near-monolayer coverages. The same mode of coordination was found for the Pt(110)-(1 × 2)-Sn surface. When the CO coverage was further increased on the Sn-free surface, an upward shift to 260 meV was observed for ν_{CO},[22] a result that served as an indicator of the presence of dipole–dipole interactions. No similar blueshift in ν_{CO} was noted on Pt(110)-(1 × 2)-Sn, most likely because CO does not bind strongly on the interfacial Sn atoms; it was noted that the coverage of CO decreased when the amount of coadsorbed Sn was increased.

3.1.2 Dioxygen

When dioxygen is chemisorbed on a transition-metal surface, an electron pair is donated from a filled 2π orbital of O_2 to a vacant $d\sigma$ orbital on the metal, followed by back-donation from a filled $d\pi$ (or $dp\pi$) metal orbital to an empty $2\pi^*$ orbital on dioxygen. As a result, the O=O bond is weakened considerably.[29–40] For example, at 100 K, chemisorption of O_2 on most metals is molecular, but the vibrational frequency of the O–O stretch mode (ν_{OO}) is drastically redshifted, 630 cm^{-1} (78.1 meV) on Ag(110),[40] 870 cm^{-1} (108 meV) on Pt(111),[38] and 850 cm^{-1} (105 meV) on Cu(111),[33] relative to that in the gas phase 1580 cm^{-1} (196 meV). At room temperature, O_2 is dissociatively chemisorbed as oxygen atoms on the same metals.

While O_2 adsorption has been investigated for a variety of substrates,[29–40] Ag and Pt have received widest attention; Ag because of its superior selectivity toward ethylene epoxidation, and Pt for its singularly high catalytic efficiency in almost all types of exhaustive oxidation reactions. The interaction of O_2 with Ag(110) was found to yield four distinct adsorption states that depended upon the temperature: a physisorbed (condensed) layer at $T < 40$ K, two molecularly chemisorbed phases between 60 K and 180 K, and a dissociatively chemisorbed (atomic) state at $T > 180$ K.[41] The first molecularly chemisorbed species, labeled α-O_2,[37] may be generated from the physisorbed state by a temperature increase to 60 K; however, α-O_2 is not dissociated to atomic oxygen at higher temperatures. It was thought that lateral interactions within the preformed physisorbed layer induced a precursor orientation that enabled conversion to α-O_2. The other molecular species, tagged as β-O_2, was formed when the Ag surface was dosed directly from the gas phase at $T > 60$; evidently, under these conditions, the physisorbed layer that is favorably oriented toward α-O_2 formation is not the initial product. Above 180 K, β-O_2 undergoes dissociative chemisorption to oxygen adatoms.

Similar results were obtained for Pt(111): four temperature-dependent adsorption states of O_2 were also formed.[38,42,43] The two molecularly chemisorbed forms identified were (i) a superoxo-type (O_2^-) species bonded at twofold bridge sites and characterized by ν_{OO} of 870 cm^{-1} (108 meV), and (ii) a peroxolike (O_2^{2-}) species more strongly coordinated ($\nu_{OO} = 690$ cm^{-1} (86 meV)) at threefold
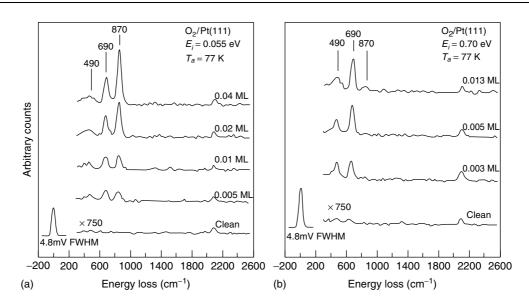
Figure 5   HREEL spectra of low-coverage doses of: (a) low incident energy (0.055 eV) oxygen, and (b) high incident energy (0.70 eV) oxygen on Pt(111) surfaces. (Reprinted with permission from P. D. Nolan, B. R. Lutz, P. L. Tanaka. J. E. Davis and C. B. Mullins. *J. Chem. Phys.* **111**:3696 (1999). © 1999 by the American Institute of Physics)

hollow sites. Experiments that combined HREELS with O_2-molecular-beam techniques indicated that high incident energies promoted the formation of the peroxo species (Figure 5a). At lower impact energies, both species were generated but the fraction of the superoxo species increased when the O_2 dosage was increased (Figure 5b). It was postulated that the O_2 molecules of higher energy are able to overcome the activation barrier for the two-electron metal-to-ligand charge transfer in the production of the peroxo species.

3.1.3   Water

As the most widely utilized solvent, studies of the adsorption of water at various surfaces abound. In such investigations, the emphasis has been on (i) its propensity toward dissociation, (ii) its structure in the adsorbed state, and (iii) its chemistry in the presence of other coadsorbed species. Although IRAS and HREELS have been employed in such studies, the former is limited to ultrathin films because of the strong infrared absorptivity of the O−H stretch mode; condensed multilayers can only be investigated by HREELS.[44]

The HREEL spectrum of water adsorbed on Pt(100) in multilayer amounts resembles that of ice. In submonolayer quantities, three ν_{OH} peaks were observed at 2850 (353 meV), 3380 (419 meV), and 3670 cm^{-1} (455 meV) respectively, these were assigned to O−H stretch modes in metal-bonded hydroxyls, hydrogen-bonded water, and water devoid of intermolecular interactions.[44] It is known that hydrogen bonding leads to a decrease in the O−H stretch frequency (ν_{OH}). When the oxygen is coordinated to the metal, the decrease in ν_{OH} is more profound. In fact, the presence of the lowest frequency ν_{OH} peak suggests that a fraction of

the adsorbed water has undergone dissociation. On Ru(0001), three ν_{OH} peaks at 2935 (364 meV), 3290 (408 meV) and 3500 cm^{-1} (434 meV) were also observed at submonolayer coverages. Unexpectedly, however, the 408-meV peak was present even when the interfacial water existed as a bilayer.[45] This result prompted the conjecture that partial decomposition had likewise taken place within the bilayer. A subsequent theoretical investigation, however, showed that the 2935 cm^{-1} peak would still be possible in a bilayer that was completely molecular; as illustrated in Figure 6,[46] two structural types of hydrogen-bonded water are possible in the bilayer.

Interfacial water was studied on Pd(100) and on Pd(100)-(1 × 1)-O surfaces. At 10 K and submonolayer coverages, the interfacial water was found to exist as monomers[47] at both surfaces. When the temperature was increased to 110 K, hydrogen-bond formation between the water molecules transpired on the clean surface but not on the oxided metal. Evidently, oxygen coadsorbed on the metal disrupted hydrogen bonding between the water molecules. Such disruption, however, does not appear to occur when the surface oxygen is part of a nonmetallic species: When water was adsorbed on ultrathin SiO_2 films, hydrogen-bonded water was observed even at submonolayer coverages; evidently, the adsorbate−adsorbate hydrogen bonds are stronger than the substrate−adsorbate interactions.[48]

The adsorption of water on Ni(100) was compared with that on Pd(110) surfaces.[49] It was noted that the Pd−OH_2 bond is substantially weaker than the Ni−OH_2 bond, a result consistent with the fact that a molecular bilayer structure is formed on Pd(110) but not on Ni(100).

Work has also been published on other interfacial materials and structures that include (i) α-Cr_2O_3(001)/α−Fe_2
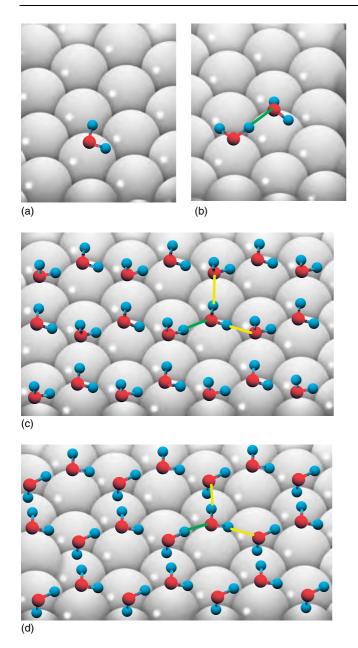
(a)

(b)

(c)

(d)

Figure 6 Equilibrium structure of (a) water monomer, (b) dimer, (c) H-up bilayer, and (d) H-down bilayer on the Pt(111) surface. (Reprinted with permission from M. Sock, A. Eichler, S. Surnev. J. N. Andersen, B. Klötzer, K. Hayek, M. G. Ramsey and F. P. Netzer. *Surf. Sci.* **545**:122 (2003). © 2003 by the American Physical Society)

$O_3/\alpha-Al_2O_3(001)$, a surface strained by the incorporation of Fe_2O_3;[50] (ii) ultrathin Pd films on MgO(100) substrates;[51] (iii) Si(100)-(2 × 1) and Si(111)-(7 × 7) single- crystal planes;[52] (iv) defect-free SrTiO$_3$(100);[53] (v) Ag(011);[54] (vi) MgO(100) superlattices on Mo(100);[55] (vii) coadsorption of CO and water on Al(111);[56] (viii) oxygen-covered Pt group metals[57,58]; and (ix) hydrogen-pretreated Pt surfaces.[59]

3.1.4 Organometallic Compounds

Interest in the structure of adsorbed organometallic compounds stems from their capabilities as research-laboratory and industrial catalysts. In view of its inherent surface sensitivity and dramatically enhanced resolution, UHREELS has recently become a viable technique in the acquisition of fingerprint spectra[60,61] of adsorbed organometallic compounds such as the metallocenes.[62–65]

Ferrocene has recently been utilized in the synthesis of carbon nanotubes.[66] In this context, HREEL spectroscopic measurements have been carried out on the adsorption of ferrocene on graphite[67]; silver substrates have also been examined.[63,68,69] On Ag(100), ferrocene was found to exist as a weakly bound molecular entity at low temperatures.[68] Loss peaks at 60.4 (487 cm^{-1}) and 93.2 meV (752 cm^{-1}) that were prominent in the HREEL spectra collected at specular angles were not observed at off-specular angles (Figure 7), a result which strongly suggests that the two loss features are exclusively dipolar in character. The peak at 60.4 meV was assigned to the antisymmetric iron–cyclopentadienyl (Fe–Cp) stretch, and the peak at 90.3 meV was ascribed to the out-of-plane C–H bend frequency, γ_{CH}.[69] For the two modes to be dipole active, both must have a vibrational-mode component that is perpendicular to the silver surface; this can be satisfied only if the ferrocene molecule is adsorbed in an ''upright'' orientation in which both Cp rings are oriented parallel to the surface (Figure 7).[63,68,69] On graphite at 140 K, a similar orientation for adsorbed ferrocene was inferred from the HREEL spectra.[67] More importantly, the frequencies of the loss peaks were found to be nearly identical to those of the gas-phase absorption peaks; the absence of adsorption-induced frequency shifts provides ample evidence that ferrocene was only physisorbed on the graphite surface.

The adsorption of iron(0) pentacarbonyl was recently studied on a Si(111)-(7 × 7) surface.[70] The interest in Fe(CO)$_5$ lies in its availability as a source gas for the chemical vapor deposition of FeSi$_2$, a critical microelectronics material.[71] Even at temperatures as low as 100 K, Fe(CO)$_5$ already underwent dissociative adsorption to yield a linear iron monocarbonyl (FeCO) surface complex. The prominent loss peaks that appeared at 53 meV (428 cm^{-1}), 81 meV (653 cm^{-1}), and 255 meV (2056 cm^{-1}) were assigned to the Si–COFe, Fe–CO, and C≡O stretch modes, respectively. These peaks were shown to arise only via dipole scattering which, because of the dipole selection rule, indicates that the adsorbed FeCO is oriented vertically with the CO moiety bonded to the Si surface.

3.1.5 Fullerene

The growth and chemistry of C$_{60}$[72] films on transition metal[73,74] and semiconductor surfaces[75–77] has been extensively studied because of potential industrial applications. The surface coordination of fullerene with
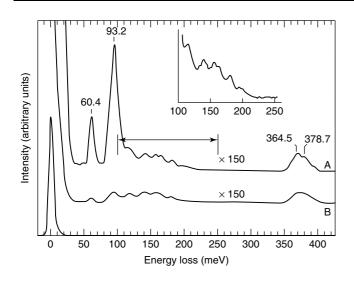
Figure 7 HREEL spectra for ferrocene adsorbed on Ag(100) at 110 K. A, specular spectrum; B, off-specular spectrum. (Reprinted with permission from Waldfried, Welipitiya, Hutchings, de Silva, Gallup, Dowben, Pai, Zhang, Wendelken and Boag.[69] © 1997 American Chemical Society)

transition-metal surfaces involves the donation of electrons from the π orbitals of the ligand to the d orbitals of the metal accompanied by the back-donation of electrons from a metal d orbital to the ligand π^* orbital. The π-electron back-donation significantly alters the chemical properties of the surface-attached C_{60}. Because of its high symmetry, there are more than just a few degenerate and IR-inactive vibrational modes.[78,79] However, most of these modes are observable in HREELS especially when detection is conducted at both specular and off-specular angles.[80]

Alkali-doped fullerides that exhibit superconductivity have received considerable attention. The spectral fingerprints of these materials show vibrational-mode-specific frequency shifts and intensity variations related to electron donation from the intercalated metal atoms to the C_{60} molecules (Figure 8a). HREELS of K-doped C_{60} thin films adsorbed on Ag(111) and Cu(111) showed loss peaks, barely visible for the undoped monolayer that increased when the dopant concentration was increased. This trend was thought to be a consequence of the charge transfer from the (electropositive) K atom to C_{60}.[81] The existence of positive K^+ ions and negative C_{60}^- ions may have been established by the appearance of a prominent optical-phonon loss peak brought about by the collective oscillations of the cations against the anions (Figure 8b).

Studies on fluoro–fullerenes ($C_{60}F_x$) were recently undertaken because of the interest in such materials as cathodes in Li batteries.[83] A recent HREELS-based work focused on the interaction between $C_{60}F_x$ and the silicon surface.[84,85] The spectrum of $C_{60}F_x$ thin layers deposited on Si(111)-(7 × 7) revealed a weak but well-defined loss feature at 107 meV. This peak was attributed to a Si–F stretch mode, which implied
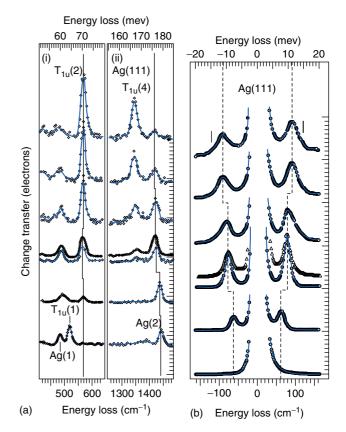

Figure 8 Evolutions of intramolecular vibrations (a) and extramolecular phonons, (b) of K-doped C_{60} on Ag(111) at different dopant concentrations. The lowest curves correspond to the undoped monolayers and the topmost ones to the saturated monolayers. (Reprinted from Silien, Thiry and Caudano,[82] © Elsevier 2004)

that the Si surface was able to defluorinate $C_{60}F_x$ and form a Si–F selvedge on the silicon substrate. The Si–F bond is rather strong and renders the substrate chemically inert toward further adsorption of $C_{60}F_x$.[84] The defluorination process is enhanced by an increase in temperature.[85]

3.2 Organic Molecules

3.2.1 Ethylene

The structure and reactivity of ethylene chemisorbed on transition-metal surfaces are of fundamental importance in surface science and heterogeneous catalysis. HREELS has been foremost among the surface characterization techniques employed; in fact, the first vibrational spectroscopic study of ethylene chemisorbed on Pt(111) was carried out with electron energy-loss spectroscopy (EELS)[86] almost a decade before IRAS was employed.[87,88]

At temperatures below 200 K, two types of ethylene-derived surface species have been identified. One is a di-σ-bonded species that results when the C=C double bond

is broken to form two C−metal bonds; the other is a π-bonded species in which the ethylene molecule remains intact. At higher temperatures, a third species, ethylidyne, may be generated on close packed face-centered cubic (111) surfaces.

The di-σ-bonded species has been observed on Pt(111),[89] Pt(100),[90] Fe(110),[91] Ru(001),[92] Si(100)[93,94] and Ni(hkl).[95–97] The HREEL spectrum of di-σ-bonded ethylene is characteristic of aliphatic (sp^3-hybridized) compounds with a C−H symmetrical stretch at ca. 3000 cm^{-1} (372 meV) and a CH$_2$ wag and C−C stretch in the region from 1170 cm^{-1} (145 meV) to 1830 cm^{-1} (227 meV); a peak near 450 cm^{-1} (55.8 meV) has been attributed to a metal−C stretch mode.[98] The π-bonded species has been found on Cu(100),[99] Pd(hkl)[100–103] as well as on hydrogen or oxygen pretreated surfaces.[104–107] The HREEL spectrum of the π-adsorbed species bears features reminiscent of the infrared spectrum of the ethylene ligand in Zeise's salt, K[(C$_2$H$_4$)PtCl$_3$][108] with the C−H symmetric stretch at 3000 cm^{-1}, and a CH$_2$ wag and the C=C stretch in the region near 1530 cm^{-1} (190 meV); the metal−C stretch was found at 300 cm^{-1} (37 meV).[98]

When either the di-σ-bonded or the π-coordinated species is warmed to room temperature, ethylidyne ($\equiv$C−CH$_3$) is generated[89,109,110]; this surface compound is rather stable since the anchored carbon is bonded to three different metal atoms. The HREEL spectrum of chemisorbed ethylidyne is characterized by vibrational modes of C_{3v} symmetry; the C−H stretch is at 2900 cm^{-1} (360 meV), the CH$_3$ wag and C−C stretch within the 1400 (174 meV) to 1800 cm^{-1} (223 meV) interval, and the M−C stretch near 425 cm^{-1}

(52.7 meV).[98] Although the complete mechanism of the ethylene to ethylidyne conversion is not known, it is thought to involve an initial dehydrogenation step followed by hydrogen migration; ethylidene (=CH−CH$_3$) was proposed as an intermediate in the transformation reaction at Pt(111).[111]

The adsorption of ethylene on clean and oxygen pretreated Pd(111) surfaces was recently studied[107]; the results in terms of HREEL spectra, are shown in Figure 9. As anticipated, ethylene was chemisorbed at 100 K as a di-σ-bonded species on the clean metal (Figure 9a). On the oxygen precoated surface, however, a π-coordinated complex was obtained (Figure 9b). At 300 K, ethylene chemisorption always resulted in an ethylidynic complex regardless of whether or not the surface was pretreated with oxygen (Figure 9c). When the di-σ-bonded or the π-attached species was warmed to 450 K, quantitative desorption of starting material (C$_2$H$_4$) occurred without dehydrogenation; no ethylidyne species was produced from either structure during the temperature increase.

Adsorption of ethylene on Rh(100) presaturated with hydrogen produced a π-bonded species at low temperatures.[105] The degree of sp^2-to-sp^3 rehybridization upon chemisorption was expressed in terms of a "$\pi\sigma$ parameter" derived from the HREEL spectrum via the mixing of the C−C (or C=C) stretch and the CH$_2$ scissor modes.[112] The $\pi\sigma$ parameter, which was normalized to zero for pure sp^2 hybridization (C$_2$H$_4$) and to unity for pure sp^3 hybridization (C$_2$H$_4$Br$_2$), was estimated to be 0.39 for chemisorbed C$_2$H$_4$; in comparison, a $\pi\sigma$ parameter of 0.38 was obtained for Zeise's salt. The close agreement

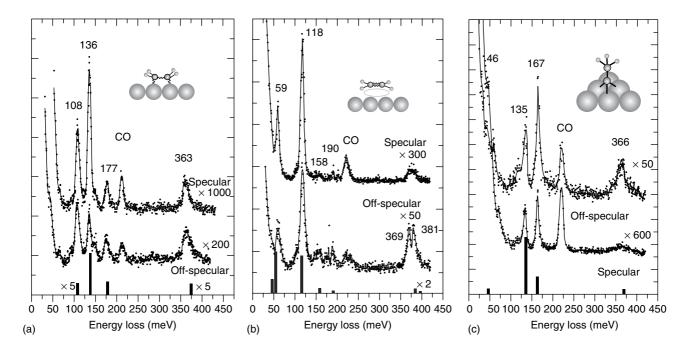**Figure 9**   Specular and off-specular HREEL spectra of (a) Pd(111) surface exposed to C$_2$H$_4$ at 100 K; (b) Pd(111)-2 × 2-O surface exposed to C$_2$H$_4$ at 100 K; and (c) Pd(111) exposed to C$_2$H$_4$ at 300 K. The bars below the spectra indicate the calculated vibrations of each species in the inset. (Reprinted from Sock, Eichler, Surnev, Andersen, Klötzer, Hayek, Ramsey and Netzer,[107] © Elsevier 2003)

between the two $\pi\sigma$ parameters provides additional evidence that the ethylene molecule is bound to the surface as a π-bonded ligand. It was also reported in the same work that an ethyl intermediate was formed from π-bonded ethylene by insertion of preadsorbed H atoms, a process that is initiated even at temperatures below 110 K. At $110\,\text{K} < T < 200\,\text{K}$, evolution of gaseous ethane was observed, but further thermal treatment resulted in the rupture of the carbon–carbon bond.

3.2.2 Methanol

Research activity on methanol has been vigorous because of its commercial importance as an alternative feedstock in fuel cells. When CH_3OH is chemisorbed on a catalytic surface at ambient temperatures, it is usually present as a methoxy intermediate; the latter then undergoes extensive decomposition to yield a product distribution that depends upon the temperature. A tabulation of products generated under various experimental conditions such as metal catalyst and decomposition temperature is given in Table 1; HREELS and temperature programmed mass spectrometry were used to generate the data.

3.2.3 Aromatic Compounds

An immediate issue in the chemisorption of aromatic compounds is whether the phenyl ring is oriented parallel or perpendicular to the plane of the metal surface. In this regard, the intensity of the out-of-plane C–H bend (γ_{CH}) relative to the in-plane C–H stretch (ν_{CH}) provides a direct diagnostic indicator of adsorbed aromatic orientation.[130–132] At specular angles, the dipole selection rule states that ν_{CH} for a ring chemisorbed completely flat would be EELS-inactive; only the γ_{CH} mode would exhibit EELS activity. At off-specular angles, the impact-scattering selection rules are less restrictive and all modes would conceivably be EELS-active, although peaks obtained at specular angles would tend to vanish as the off-specular angle φ is increased.

Early studies with smooth polycrystalline Pt electrodes indicated that aromatic compounds such as p-diphenols

Table 1 Methanol decomposition on various metal surfaces

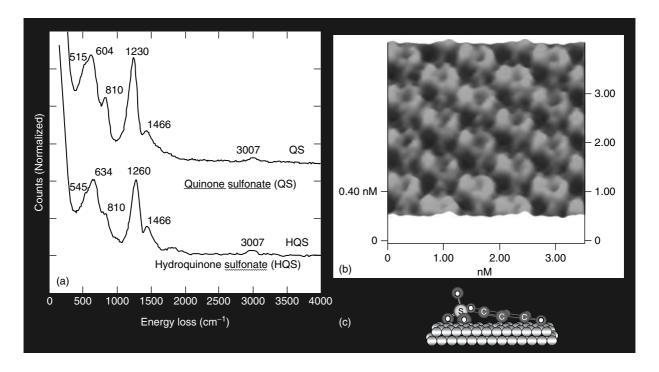| Surface	Temperature (K)	Decomposition/chemisorption products	References
V(110)	100	Methoxy ($-O-CH_3$)	113
C-modified V(110)	100	$-O-CH_3$	113
Ti(0001)	100	$-O-CH_3$	113
C-modified Ti(0001)	100	$-O-CH_3$	113
S-modified Fe(100)	150	CH_3O-(decreases if S is increased)	114
	450	CO (decreases if S is increased)	114
Fe(100)	110	CH_3O-	114
	450	H_2 and CO	114
O-modified Fe(100)	150	$-O-CH_3$	115
Pt(111)	200	CO and H	116
Pt(100)	200	H and CO	117
Pt(110)	140	$-CH_x$	118
	250	CH_4, H and C	118
Pt(110)-(2 × 1)	130	$-O-CH_3$	118
	250	CO and H	115
Rh(100)	250	$-O-CH_3$	119
	320	CO and H	119
Rh(111)	140	$-O-CH_3$	120
	210	CO and H_2	120
O-modified Rh(111)	140	$-O-CH_3$	120
Ni(110)	170	$-O-CH_3$	121
	270	CO and H	121
Ru(0001)	300	CO and H	122
Pd(111)	300	CO	123
Pd(100)	77	Methoxide (CH_3O^-)	124
	530	CO, H and H_2	124
Ge	300	$-CH_3$ and $-OH$	125
NiAl(100)	120	$-O-CH_3$	126
	400	H_2, CH_4, $-CH_3$ and C_2H_4	126
NiAl(110)	120	$-O-CH_3$	126
	400	H_2, CO, CH_4, $-CH_3$ and C_2H_4	114
NiAl(111)	200	$-O-CH_3$	127
	650	H_2, CO, CH_4, and CH_3	127
Cu(100)	370	Unidentified gaseous products	128
Co-modified Mo(110)	250	CH_3O^-	129

Figure 10 HREEL spectrum (a), in situ scanning tunneling microscope image (b), and molecular model (c) of quinone sulfonate chemisorbed on Pd(100)

are chemisorbed in discrete, nonrandom orientations that depend upon interfacial factors such as the solution concentration of the aromatic and the composition of the supporting electrolyte.[133–135] For example, when chemisorbed from dilute (0.1 mM) solutions, a molecular layer of horizontally oriented (η^6-coordinated) quinonoid species is formed; at higher concentrations (2 mM), a layer of vertically oriented (2,3-η^2-bound) aromatic molecules is generated. The orientational assignments made from measured adsorbed-molecule cross sections have since been verified by independent experiments foremost of which has been HREELS; work with the diphenols has been carried out with Pt and Pd single crystals.[136–139]

Figure 10 shows HREEL spectra of a Pd(111) electrode emersed[e] from aqueous solutions that contained either 0.1 mM hydroquinone sulfonate or 0.1 mM benzoquinone sulfonate.[132] Four features are most notable: (i) the spectra are identical whether the starting material is the diphenol or the quinone; (ii) there is a pronounced out-of-plane C−H bend (γ_{CH}) at 810 cm^{-1} (100 meV); (iii) no O−H stretch (ν_{OH}) is observed near 3600 cm^{-1} (446 meV); and (iv) there is a small but noticeable in-plane C−H stretch (ν_{CH}) at 3007 cm^{-1} (373 meV). These results indicate that, upon surface coordination, the diphenolic species undergoes a two-electron, two-proton oxidation to form essentially flat-chemisorbed benzoquinone; the small ν_{CH} peak, however, indicates that the aromatic ring is not completely flat, but is slightly tilted. The combination of HREELS and electrochemical (in situ) scanning tunneling microscopy[140] has been used to deduce the adsorbed−molecule orientation of the sulfonated quinone

(Figure 10). Recent HREELS and thin-layer electrochemical measurements[141] have demonstrated that, at a tenfold increase in solution concentration, hydroquinone is chemisorbed on Pd(111) in an edgewise orientation reminiscent of an *o*-benzyne organometallic complex.[133–135]

The desorption and decomposition of benzene has been studied on Pt(111) and on Sn-modified Pt(111) for comparative purposes.[142] On the former surface, only a portion of the chemisorbed benzene desorbs upon heat treatment; the remainder is dehydrogenated to form a layer of carbon on the surface. On the Pt(111)-Sn alloys, only physisorption takes place.

The cyclization reaction of acetylene at ambient temperatures to form benzene on Pd(111) has recently been reinvestigated in an attempt to gain insights into its mechanism.[143] It has been claimed that, at low exposures of acetylene, only ethylidyne is formed. At higher exposures, benzene is formed, albeit at low coverages, as indicated by appearance of the ν_4 band of benzene at 720 cm^{-1}.

More recent work on the chemisorption of aromatic molecules has focused on new materials (e.g., Mo(112)-c(2 × 2)-SiO$_2$ and Mo$_2$C/Mo(100)) and with various benzene derivatives (e.g., C$_6$H$_5$I and C$_5$NH$_5$).[144–147]

3.2.4 Polymers

Only feeble attempts were initially made two decades ago in the application of HREELS to the study of polymer surfaces. The efforts did not become more earnest until a

decade later. The use of HREELS has primarily been focused on the following aspects related to polymer films deposited on metals as well as to surfaces of the polymer films themselves: surface morphology, interfacial composition, the scattering mechanism, and the strength of the polymer–substrate bond. The utility of HREELS to probe polymer-surface morphology rests on the observation that elastic peaks due to electrons backscattered from hydrogen atoms can be correlated with the hydrogen content at smooth surfaces.[148]

Systems that employed HREELS for interfacial-composition determinations included: poly(ethylene oxide)-polystyrene diblock copolymer on Si wafers[149]; formaldehyde poly(oxymethylene) films on Cu(100)[150]; and Langmuir–Blodgett films of 4,4'-oxydianiline-pyromellitic dianhydride polyimide on Au and on highly ordered pyrolytic graphite.[151]

HREELS experiments with bisphenol-A polycarbonate, high-density polyethylene, and poly(2-vinylpyridine) suggested that, although dipole and impact scattering are prominent in polymer films, negative-ion resonance scattering cannot be discounted.[152] Investigations with highly oriented poly(tetrafluoroethylene) likewise indicated appreciable negative-ion resonance impact scattering with a maximum cross section at an incident electron energy of around 4 eV.[153]

The use of vibrational spectroscopy to monitor the strength of polymer adhesion on foreign substrates is based upon adsorption-induced frequency shifts and intensity changes in the free polymer modes and the emergence of new spectral peaks; the latter, due to metal–polymer bonds, generally appear at energies lower than 75 meV that can be accessed only by HREELS. It was found, for example, that Pd is inert toward polyimide, but Cr is quite reactive.[154] The interaction between aluminum deposited onto a polyimide film was also investigated by HREELS. When the Al coverage was $< 10^{14}$ atoms cm^{-2}, the reaction was limited to Al with the carbonyl group to form a C–O–metal complex. At a twofold increase in coverage, Al–O and Al–C bonds were formed; at intermediate coverages, no polymer–Al reactions transpired but bond breaking processes in the polymer occurred.[155]

3.2.5 Self-Assembled Monolayers

Technological and scientific interest in self-assembled monolayers (SAMs) lie in their applicability in many areas such as corrosion protection, biomimetic membranes, and chemical sensors.[156] The driving force in the facile formation of SAMs is the high affinity of an end group for the metal substrate. Organosulfur compounds such as alkanethiol and dialkyl disulfides have been widely studied because they spontaneously form highly ordered structures on transition-metal surfaces such as Au and Pt. IRAS, Raman scattering, sum-frequency generation and HREELS are among the vibrational spectroscopy techniques employed to probe the structure and organization of monolayer and bilayer SAMs.[157] HREELS has the unique advantage in that the metal–sulfur

stretch mode occurs at low frequencies inaccessible by the other methods; hence, a determination of the adsorption sites of the organosulfur compounds is possible only with HREELS.[158,159] In addition, the degree of order in SAMs can be addressed uniquely by HREELS via a comparison of the specular and off-specular HREEL spectra.[160]

A vast majority of HREELS work has been focused on Au(111) and Au(100) surfaces.[161–163] The HREEL spectrum of alkanethiols surface coordinated on Au can be divided into the following group-frequency regions: 200 (24.8 meV) to 360 cm^{-1} (44.6 meV) for the Au–S stretch region; 620 (77 meV) to 740 cm^{-1} (91.7 meV) for the C–S stretch region; 1000 (124 meV) to 1100 cm^{-1} (136 meV) for the C–C stretch region; 1200 (149 meV) to 3000 cm^{-1} (372 meV) for the C–H stretch region; and 700 (86.9 meV) to 900 cm^{-1} (112 meV) for the C–H wag region). The absence of an S–H peak in the spectrum indicates that alkanethiol chemisorption involves the loss of an S–H bond to form an M–S bond accompanied by the evolution of H_2 gas.

The effect of alkyl chain length on the structure of alkanethiols on Au(111) was studied with $CH_3(CH_2)_{n-1}SH$, where $n = 2, 4, 6, 8, 10, 11, 12, 14, 15, 16,$ and 18.[164] The results, in terms of HREEL spectra, are displayed in Figure 11. It is most interesting to note that the intensity of CH_3 σ-deformation mode at 1380 cm^{-1} (171 meV) is profoundly dependent on the number of carbons in the alkyl chain: It is present only when the number of carbon atoms is even (cf., the spectra labeled C_{10}, C_{12} and C_{16}); it is absent when the number is odd (cf., the spectra labeled C_{11} and C_{15}). This "odd–even" trend is caused by the fact that the orientation of the CH_3 head is parallel to the surface for odd number of carbon atoms but perpendicular when the number is even (cf., the inset in Figure 11). As dictated by the dipole selection rules, only the oscillator that has a component perpendicular to the surface (as in the even number chain) would show HREELS activity. It can also be seen in the frequency region below 220 cm^{-1} (27.3 meV) that more than one peak, separated by about 30 cm^{-1} (3.7 meV) are present; this indicates the existence of multiple adsorption sites for the subject alkanethiols on Au(111).

Octanethiol SAMs on Au(111) have been found to undergo an adlattice transition from a c(4 × 2) to a (6 × $\sqrt{3}$) structure after long-term storage. HREELS was one of the techniques employed to examine the cause for the transitions.[165] It was established that the structural transitions were caused by the dynamic surface diffusion of the sulfur anchor group between multiple adsorption sites. The adsorption-site exchange also resulted in orientational changes in alkyl chains.[164]

The properties of octadecanethiol SAMs on three different gold substrates, Au on Si, Au(111), and Au(100), were studied by HREELS for comparative purposes.[132,140,141] The angular distribution of the elastic peak from the SAM on the Au on Si film was found to be at least 5 times broader than those on Au(111) and Au(100). This suggests
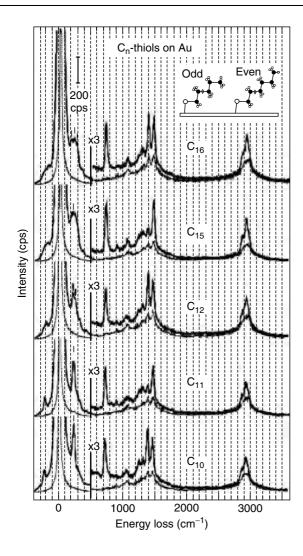
Figure 11 Odd–even effect on HREEL spectra of various alkanethiol SAMs on Au. The specular spectra and the off-specular spectra were plotted as solid and dotted lines, respectively. (Reprinted with permission from Kato, Noh, Hara and Kawai.[158] © 2002 American Chemical Society)

that the SAM on the Au film was far less ordered than on Au(111) and Au(100). An analysis of the dipole scattering and impact scattering contributions to the HREEL spectra provided evidence that the CH_2 (rocking and scissoring) and CH_3 (bending) modes are predominantly dipole scatterers, whereas the C–C and C–H stretching modes are primarily impact scatterers.[165]

Thiophenols and thiophenol derivatives chemisorbed on well-defined electrode surfaces have also been studied by HREELS.[2] The cyclic voltammetric peaks for the quinone/hydroquinone redox reaction of the 2,5-dihydroxythiophenol immobilized on the Pt surface was much broader than for the unadsorbed species; the broadening vanished when a methylene group was placed between the —SH group and the phenyl ring. These results indicated strong substrate mediated adsorbate–adsorbate interactions. Such

interactions, however, were not manifested in the HREEL spectrum. This suggested that the adsorbate–adsorbate interactions were purely electronic in nature, devoid of vibrational (or vibronic) perturbations.

4   ACKNOWLEDGMENTS

5   ABBREVIATIONS AND ACRONYMS

EELS = electron energy-loss spectroscopy; HR-EEL = high-resolution electron energy-loss; HREELS = high-resolution electron energy-loss spectroscopy; UHRE-ELS = ultrahigh-resolution electron energy-loss spectroscopy; IRAS = infrared reflection-absorption spectroscopy; SAMs = self-assembled monolayers; UHV = ultrahigh vacuum; Cp = cyclopentadienyl group φ = off-specular scattering angle.

6   END NOTES

a. $1\,eV = 8066\,cm^{-1} = 96.48\,kJ\,mol^{-1}$.

b.   HREELS generally does not possess enough sensitivity to detect higher-order effects due to mechanical and/or electrical anharmonicity.

c.   In IRAS, the surface is irradiated at near-grazing incidence and the quantity of absorption is obtained from the attenuation of the intensity of the reflected beam. Adsorbed molecule orientation can be determined directly from the spectrum since the metal–surface dipole selection rule states that only vibrations with components perpendicular to the surface are active.

d.   A third mechanism, first observed in gas-phase electron-impact scattering, has been referred to as negative-ion resonance. In this process, an electron is trapped, within 10^{-15} s, inside the molecule in a negative-ion state. For chemisorbed molecules, however, the adsorbate-substrate chemical bond and the electron–surface interactions can dramatically alter the resonance properties.[6] Hence, for HREELS at metal surfaces, this mechanism is quite rare; it will not be treated further in this article.

e.   In electrochemical surface science, emersion is a term used to indicate the removal of an electrode from solution under potential control.

7 FURTHER READING

F. Allegretti, V. De Renzi, R. Biagi, U. del Pennino, G. Contini, V. Di Castro, C. Mariani and C. Fontanesi, *Surf. Sci.*, 2003, **539**, 63.

J. M. Auerhammer, M. Knupfer, H. Peisert and J. Fink, *Surf. Sci.*, 2002, **506**, 333.

A. Bansal, Xiuling. Li, Sang. I. Yi, W. H. Weinberg and N. S. Lewis, *J. Phys. Chem.*, 2001, **105**, 10266.

W. Chen, I. Ermanoski, Q. Wu, T. E. Madey, H. H. Hwu and J. G. Chen, *J. Phys. Chem.*, 2003, **107**, 5231.

Y. Chen, R. E. Palmer and J. P. Wilcoxon, *Surf. Sci.*, 2000, **454–456**, 963.

M. S. Chen, A. K. Santra and D. W. Goodman, *J. Phys. Chem.*, 2004, **108**, 17940.

T. V. Choudhary and D. W. Goodman, *Top. Catal.*, 2002, **20**, 35.

V. De Renzi, R. Biagi and U. del Pennino, *Phys. Rev. B*, 2001, **64**, 1.

S. V. Didziulis, P. Frantz, L. C. Fernandez-Torres, R. L. Guenard and S. S. Perry, *J. Phys. Chem.*, 2001, **105**, 5196.

A. -S. Duwez, *J. Electron Spectrosc. Relat. Phenom.*, 2004, **134**, 97.

Y. Fukuda, T. Kobayashi, H. Yoshida, T. Sekizawa and N. Sanada, *Appl. Surf. Sci.*, 2002, **190**, 279.

V. V. Gorodetskii, M. Yu. Smirnov and A. R. Cholach, *Stud. Surf. Sci. Catal.*, 1993, **75**, 1587.

C. J. Hagedorn, M. J. Weiss and W. H. Weinberg, *J. Phys. Chem.*, 2001, **105**, 3838.

R. D. Haley, M. S. Tikhov and R. M. Lambert, *Catal. Lett.*, 2001, **76**, 125.

G. Hamm, T. Schmidt, J. Breitbach, D. Franke, C. Becker and K. Wandelt, *Surf. Sci.*, 2004, **562**, 170.

M. A. Henderson and S. A. Chambers, *Surf. Sci.*, 2000, **449**, 135.

G. Hess, Ch. Baumgartner and H. Froitzheim, *Phys. Rev. B*, 2001, **63**, 1.

T. Hoeche, F. Heyroth, M. Grodzicki and P. A. van Aken, *Phys. Status Solidi A*, 2005, **202**, 2355.

K. Jacobi, Y. Wang, C. Y. Fan and H. Dietrich, *J. Chem. Phys.*, 2001, **115**, 4306.

I. Jungwirthova and L. L. Kesmodel, *Surf. Sci.*, 2000, **470**, L39.

S. Katano, H. S. Kato, M. Kawai and K. Domen, *J. Phys. Chem.*, 2003, **107**, 3671.

K. A. Layman, M. M. Ivey and J. C. Hemminger, *J. Phys. Chem.*, 2003, **107**, 8538.

J. P. Lu, M. R. Albert and S. L. Bernasek, *Surf. Sci.*, 1991, **258**, 269.

K. K. Meagher, A. B. Bocarsly, S. L. Bernasek and T. A. Ramanarayanan, *J. Phys. Chem.*, 2000, **104**, 3320.

U. A. Paulus, Y. Wang, H. P. Bonzel, K. Jacobi and G. Ertl, *J. Phys. Chem.*, 2005, **109**, 2139.

V. M. Rei, P. Lang, G. Horowitz, C. Nogues, Y. Jugnet, O. Pellegrino and A. M. Botelho do Rego, *Langmuir*, 2003, **19**, 2649.

T. J. Rockey, M. Yang and H. L. Dai, *Surf. Sci.*, 2005, **589**, 42.

E. Salomon, T. Angot, N. Papageorgiou and J. -M. Layet, *Surf. Sci.*, 2005, **596**, 74.

C. Silien, Y. Caudano, A. Peremans and P. A. Thiry, *Appl. Surf. Sci.*, 2000, **162**, 445.

C. Silien, P. A. Thiry and Y. Caudano, *Phys. Rev. B*, 2003, **67**, 075412.

M. Sock, A. Eichler, S. Surnev, J. N. Andersen, B. Klotzer, K. Hayek, M. G. Ramsey and F. P. Netzer, *Surf. Sci.*, 2003, **545**, 122.

P. J. Unwin and T. S. Jones, *Surf. Sci.*, 2003, **532**, 1011.

J. Wang, C. Y. Fan, Q. Sun, K. Reuter, K. Jacobi, M. Scheffler and G. Ertl, *Angew. Chem.*, 2003, **42**, 2151.

C. M. Whelan, F. Cecchet, G. J. Clarkson, D. A. Leigh, R. Caudano and P. Rudolf, *Surf. Sci.*, 2001, **474**, 71.

X. Yang, Z. H. He, X. J. Zhou, S. H. Xu and K. T. Leung, *Appl. Surf. Sci.*, 2006, **252**, 3647.

H. Zhao, J. Kim and B. E. Koel, *Surf. Sci.*, 2003, **538**, 147.

8 REFERENCES

1. G. A. Somorjai, 'Introduction to Surface Chemistry and Catalysis', John Wiley & Sons, New York, 1994.

2. G. Ertl and J. Kuppers, 'Low Energy Electrons and Surface Chemistry', VCH Publishers, Weinheim, 1985.

3. H. Froitzheim, in 'Topics in Current Physics', ed. H. Ibach, Springer-Verlag, New York, 1977.

4. H. Ibach and D. L. Mills, 'Electron Energy Loss Spectroscopy and Surface Vibrations', Academic Press, New York, 1982.

5. N. R. Avery, in 'Vibrational Spectroscopy of Molecules on Surfaces', eds. J. T. Yates, Jr and T. E. Madey, Plenum Press, New York, 1987.

6. L. L. Kesmodel, in 'Surface Imaging and Visualization', ed. A. T. Hubbard, CRC Press, Boca Raton, 1995.

7. http://www.lktech.com/products/els5000.php, 2006.

8. J. E. Soto-Chevres, Molecular Adsorption at Well-Defined Palladium Electrode Surfaces, Ph. D. Dissertation, Texas A&M University, College Station, 2000.

9. F. A. Cotton and G. Wilkinson, 'Advanced Inorganic Chemistry', Wiley-Interscience, New York, 1988.

10. G. Blyholder, *J. Phys. Chem.*, 1964, **68**, 2772.

11. N. Sheppard and T. T. Nguyen, in 'Advances in Infrared and Raman Scattering', eds. R. E. Hester and R. J. H. Clark, Hayden and Son, London, 1978.

12. W. Erley, H. Wagner and H. Ibach, *Surf. Sci.*, 1979, **80**, 612.

13. V. Formoso, A. Marino, G. Chiarello, R. G. Agostino, T. Caruso and E. Colavita, *Surf. Sci.*, 2006, **600**, 1456.

14. H. S. Kato, H. Okuyama, J. Yoshinobu and M. Kawai, *Surf. Sci.*, 2002, **513**, 239.

15. H. Steininger, S. Lehwald and H. Ibach, *Surf. Sci.*, 1982, **123**, 264.

16. J. Wang, Y. Wang and K. Jacobi, *Surf. Sci.*, 2001, **482**, 153.

17. J. Radnik and H. J. Ernst, *J. Chem. Phys.*, 1999, **110**, 10522.

18. D. L. S. Nieskens, M. M. M. Jansen, A. P. Van Bavel, D. Curulla-Ferre and J. W. Niemantsverdriet, *Phys. Chem. Phys.*, 2006, **8**, 624.

19. A. G. Baca, L. E. Klebanoff, M. A. Schulz, D. Paparazzo and D. A. Shirley, *Surf. Sci.*, 1986, **173**, 215.

20. M. L. Colaianni, J. G. Chen, W. H. Weinberg and J. T. Yates, Jr, *J. Am. Chem. Soc.*, 1992, **114**, 3735.

21. C. M. Friend, J. G. Serafin, E. K. Baldwin, P. A. Stevens and R. J. Madix, *J. Chem. Phys.*, 1987, **87**, 1847.

22. H. Von Schenck, E. Janin, O. Tjernberg, M. Svensson and M. Gothelid, *Surf. Sci.*, 2003, **526**, 184.

23. C. Lemire, R. Meyer, V. E. Henrich and H. J. Freund, *Surf. Sci.*, 2004, **572**, 103.

24. S. H. Kim, U. A. Paulus, Y. Wang, J. Wintterlin, K. Jacobi and G. Ertl, *J. Chem. Phys.*, 2003, **119**, 9729.

25. H. Hopster and H. Ibach, *Surf. Sci.*, 1978, **77**, 109.

26. S. R. Bare, P. Hofmann and D. A. King, *Surf. Sci.*, 1984, **144**, 347.

27. Z. Chen, D. H. Gracias and G. A. Somorjai, *Appl. Phys. B*, 1999, **68**, 549.

28. R. Linke, D. Curulla, M. J. P. Hopstaken and J. W. Niemantsverdriet, *J. Chem. Phys.*, 2001, **115**, 8209.

29. Y. C. Lee and P. A. Montano, *Surf. Sci.*, 1985, **149**, 471.

30. T. S. Rahman, A. B. Anton, N. R. Avery and W. H. Weinberg, *Phys. Rev. Lett.*, 1983, **51**, 1979.

31. N. D. Shinn and T. E. Madey, *Surf. Sci.*, 1986, **173**, 379.

32. S. H. Kim and P. C. Stair, *Surf. Sci.*, 2000, **457**, L347.

33. T. Sueyoshi, T. Sasaki and Y. Iwasawa, *Surf. Sci.*, 1996, **365**, 310.

34. C. de Verdiere, J. Szeftel and P. Soukiassian, *Phys. Rev. B*, 1990, **42**, 7234.

35. F. P. Leisenberger, G. Koller, M. Sock, S. Surnev, M. G. Ramsey, F. P. Netzer, B. Klotzer and K. Hayek, *Surf. Sci.*, 2000, **445**, 380.

36. P. D. Nolan, B. R. Lutz, P. L. Tanaka, J. E. Davis and C. B. Mullins, *J. Chem. Phys.*, 1999, **111**, 3696.

37. F. Bartolucci, R. Franchy, J. C. Barnard and R. E. Palmer, *Phys. Rev. Lett.*, 1998, **80**, 5224.

38. J. L. Gland, B. A. Sexton and G. B. Fisher, *Surf. Sci.*, 1980, **95**, 587.

39. H. Steininger, S. Lehwald and H. Ibach, *Surf. Sci.*, 1982, **123**, 1.

40. C. Backx, C. P. M. De Groot and P. Biloen, *Surf. Sci.*, 1981, **104**, 300.

41. K. C. Prince, G. Paolucci and A. M. Bradshaw, *Surf. Sci.*, 1986, **175**, 101.

42. D. H. Parker, M. E. Bartram and B. E. Koel, *Surf. Sci.*, 1989, **217**, 489.

43. K. Gustafsson and S. Andersson, *J. Chem. Phys.*, 2004, **120**, 7750.

44. H. Ibach and S. Lehwald, *Surf. Sci.*, 1980, **91**, 187.

45. P. A. Thiel, R. A. Depaola and F. M. Hoffmann, *J. Chem. Phys.*, 1984, **80**, 5326.

46. S. Meng, L. F. Xu, E. G. Wang and S. Gao, *Phys. Rev. Lett.*, 2002, **89**, 176104.

47. C. T. Nyberg, C. G. Tengstal, P. Uvdal and S. Andersson, *J. Electron Spectrosc. Relat. Phenom.*, 1986, **38**, 299.

48. S. F. Wendt, T. Wei, M. S. Chen, V. Kempter and D. W. Goodman, *Surf. Sci.*, 2004, **565**, 107.

49. R. B. Rosseau and T. H. Ellis, *Surf. Sci.*, 1993, **280**, 23.

50. M. A. Henderson and S. A. Chambers, *Surf. Sci.*, 2000, **449**, 135.

51. F. Xu, Q. Guo and P. Moller, *J. Phys. Chem. B*, 2005, **109**, 9517.

52. H. W. Ibach, H. Wagner and D. Bruchmann, *Solid State Commun.*, 1982, **42**, 457.

53. P. A. E. Cox and P. D. Naylor, *J. Electron Spectrosc. Relat. Phenom.*, 1983, **29**, 247.

54. K. J. Wu, G. S. Elliott and S. D. Kevan, *J. Chem. Phys.*, 1989, **91**, 7964.

55. Y. Yu, Q. Guo, S. Liu, E. Wang and P. Moller, *Phys. Rev. B*, 2003, **68**, 115414.

56. K. B. Jacobi, P. Geng, W. Hansen, J. Schreiner and C. Astaldi, *Surf. Sci.*, 1991, **245**, 72.

57. E. Stuve and R. J. Madix, *Surf. Sci.*, 1984, **146**, 179.

58. M. S. Hock, I. Bassignana, K. Wagemann and J. Kueppers, *Surf. Sci.*, 1986, **177**, L978.

59. N. B. Chen and R. I. Masel, *Surf. Sci.*, 1999, **419**, 150.

60. G. Davidson, *Spectrosc. Prop. Inorg. Organomet. Compd.*, 1985, **18**, 220.

61. S. Cradock, *Spectrosc. Prop. Inorg. Organomet. Compd.*, 1985, **17**, 184.

62. D. L. Pugmire, C. M. Woodbridge, N. M. Boag and M. A. Langell, *Surf. Sci.*, 2001, **472**, 155.

63. C. M. Woodbridge, D. L. Pugmire, R. C. Johnson, N. M. Boag and M. A. Langell, *J. Phys. Chem. B*, 2000, **104**, 3085.

64. C. F. McConville and T. S. Jones, *Surf. Sci.*, 2002, **515**, 403.

65. Y. Fukuda, T. Kobayashi, H. Yoshida, T. Sekizawa and N. Sanada, *Appl. Surf. Sci.*, 2002, **190**, 279.

66. R. Sen, A. Govindaraj and C. N. R. Rao, *Chem. Phys. Lett.*, 1997, **267**, 276.

67. P. J. Durston and R. E. Palmer, *Surf. Sci.*, 1998, **400**, 277.

68. D. Welipitiya, P. A. Dowben, J. Zhang, W. W. Pai and J. F. Wendelken, *Surf. Sci.*, 1996, **367**, 20.

69. C. Waldfried, D. Welipitiya, C. W. Hutchings, H. S. V. de Silva, G. A. Gallup, P. A. Dowben, W. W. Pai, J. Zhang, J. F. Wendelken and N. M. Boag, *J. Phys. Chem. B*, 1997, **101**, 9782.

70. S. Mülbauer, A. Petkova and H. Froitzheim, *Surf. Sci.*, 2004, **562**, 195.

71. B. Rösen, H. Ch. Schäfer, Ch. Dieker, L. Lüth, A. Rizzi and D. Gerthsen, *J. Vac. Sci. Technol., B*, 1993, **11**, 1407.

72. H. W. Kroto, J. R. Heath, S. C. O'Brian, R. F. Curl and R. E. Smalley, *Nature*, 1985, **318**, 162.

73. A. Sellidj and B. E. Koel, *J. Phys. Chem.*, 1993, **97**, 10076.

74. C. Silien, I. Marenne, J. Auerhammer, N. Tagmatarchis, K. Prassides, P. A. Thiry and P. Rudolf, *Surf. Sci.*, 2001, **482**, 1.

75. G. Gensterblum, L. M. Yu, J. J. Pireaux, P. A. Thiry, R. Caudano, Ph. Lambin, A. A. Lucas, W. Krätschmer and J. E. Fischer, *J. Phys. Chem. Solids*, 1992, **53**, 1427.

76. P. Dumas, M. Gruyters, P. Rudolf, Y. He, L. -M. Yu, G. Gensterblum, R. Caudano and Y. J. Chabal, *Surf. Sci.*, 1996, **368**, 330.

77. S. Suto, K. Sakamoto, D. Kondo, T. Wakita, A. Kimura, A. Kakizaki, C. -W. Hu and A. Kasuya, *Surf. Sci.*, 1999, **438**, 242.

78. H. Kuzmany, R. Winkler and T. Pichler, *J. Phys.: Condens. Matter*, 1995, **7**, 6601.

79. H. Kuzmany, M. Matus, B. Burger and J. Winter, *Adv. Mater.*, 1994, **6**, 731.

80. G. Gensterblum, J. J. Pireaux, P. A. Thiry, R. Caudano, J. P. Vigneron, Ph. Lambin and A. A. Lucas, *Phys. Rev. Lett.*, 1991, **67**, 2171.

81. W. Andreoni, P. Giannozzi and M. Parrinello, *Phys. Rev. B* 1995, **51**, 2087.

82. C. Silien, P. A. Thiry and Y. Caudano, *Surf. Sci.*, 2004, **558**, 174.

83. T. Nakajima, B. Zemva and A. Tressaud, 'Advanced Inorganic Fluorides: Synthesis, Characterization and Applications', Elsevier, St. Louis, 2000.

84. J. T. Sasowski, Y. Fujikawa, K. F. Kelly, K. Nakayama, T. Sakurai, E. T. Mickelson, R. H. Hauge and J. L. Margrave, *J. Cryst. Growth*, 2001, **229**, 580.

85. J. T. Sasowski, Y. Fujikawa, K. F. Kelly, K. Nakayama, T. Sakurai, E. T. Mickelson, R. H. Hauge and J. L. Margrave, *Mater. Charact.*, 2002, **48**, 127.

86. H. Ibach and S. Lehwald, *J. Vac. Sci. Technol.*, 1978, **15**, 407.

87. M. A. Chesters and E. M. McCash, *Surf. Sci.*, 1987, **187**, L639.

88. I. J. Malik, M. E. Brubaker, S. B. Mohsin and M. Trenary, *J. Chem. Phys.*, 1987, **87**, 5554.

89. H. Steininger, H. Ibach and S. Lehwald, *Surf. Sci.*, 1982, **117**, 685.

90. G. H. Hatzikos and R. I. Masel, *Surf. Sci.*, 1987, **185**, 479.

91. W. Erley, A. M. Baro and H. Ibach, *Surf. Sci.*, 1982, **120**, 273.

92. M. A. Barteau, J. Q. Broughton and D. Menzel, *Appl. Surf. Sci.*, 1984, **19**, 92.

93. J. Yoshinobu, H. Tsuda, M. Onchi and M. Nishijima, *Solid State Commun.*, 1986, **60**, 801.

94. C. Huang, W. Widdra and W. H. Weinberg, *Surf. Sci.*, 1994, **315**, L953.

95. L. Hammer, T. Hertlein and K. Müller, *Surf. Sci.*, 1986, **178**, 693.

96. S. Lehwald, H. Ibach and H. Steininger, *Surf. Sci.* 1982, **117**, 342.

97. C. E. Anson, B. J. Bandy, M. A. Chesters, B. Keiller, I. A. Oxton and N. Sheppard, *J. Electron Spectrosc. Relat. Phenom.*, 1983, **29**, 315.

98. N. Sheppard, *Annu. Rev. Phys. Chem.*, 1988, **39**, 589.

99. C. Nyberg, C. G. Tengstål, S. Andersson and M. W. Holmes, *Chem. Phys. Lett.*, 1982, **87**, 87.

100. J. A. Gates and L. L. Kesmodel, *Surf. Sci.*, 1985, **120**, L461.

101. J. A. Gates and L. L. Kesmodel, *Surf. Sci.*, 1985, **124**, 68.

102. M. A. Chesters, G. S. McDougall, M. E. Pemble and N. Sheppard, *Appl. Surf. Sci.*, 1985, **22**, 369.

103. H. Okuyama, S. Ichihara, H. Ogasawara, H. Kato, T. Komeda, M. Kawai and J. Yoshinobu, *J. Chem. Phys.*, 2000, **112**, 5948.

104. S. Ichihara, H. Okuyama, H. Kato, M. Kawai and K. Domen, *Chem. Lett.*, 2000, **2**, 112.

105. C. Egawa, *Surf. Sci.*, 2000, **454**, 222.

106. E. M. Stuve and R. J. Madix, *Surf. Sci.*, 1985, **160**, 293.

107. M. Sock, A. Eichler, S. Surnev, J. N. Andersen, B. Klötzer, K. Hayek, M. G. Ramsey and F. P. Netzer, *Surf. Sci.*, 2003, **545**, 122.

108. M. J. Grogan and K. Nakamoto, *J. Am. Chem. Soc.*, 1966, **88**, 5454.

109. J. A. Gates and L. L. Kesmodel, *Surf. Sci.*, 1982, **120**, L461.

110. J. A. Gates and L. L. Kesmodel, *Surf. Sci.*, 1983, **124**, 68.

111. C. Hwang, C. Lee, H. Kang and C. Kim, *Surf. Sci.*, 2001, **490**, 144.

112. E. M. Stuve, R. J. Madix and C. R. Brundle, *Surf. Sci.*, 1985, **152**, 532.

113. M. B. Zellner, H. H. Hwu and J. G. Chen, *Surf. Sci.*, 2005, **598**, 185.

114. J. P. Lu, M. R. Albert and S. L. Bernasek, *Surf. Sci.*, 1991, **258**, 269.

115. J. P. Lu, M. Albert, S. L. Bernasek and D. Dwyer, *Surf. Sci.*, 1989, **218**, 1.

116. K. D. Gibson and L. H. Dubois, *Surf. Sci.*, 1990, **233**, 59.

117. N. Kizhakevariam and E. M. Stuve, *Surf. Sci.*, 1993, **286**, 246.

118. J. Wang and R. I. Masel, *J. Vac. Sci. Technol., A*, 1991, **9**, 1879.

119. J. E. Parmeter, X. Jiang and D. W. Goodman, *Surf. Sci.*, 1990, **240**, 85.

120. C. Houtman and M. Barteau, *Langmuir*, 1990, **6**, 1558.

121. L. J. Richter and W. Ho, *J. Chem. Phys.*, 1985, **83**, 2569.

122. J. Hrbek, R. A. DePaola and F. M. Hoffmann, *J. Chem. Phys.*, 1984, **81**, 2818.

123. J. A. Gates and L. L. Kesmodel, *J. Catal.*, 1983, **83**, 437.

124. K. Christmann and J. E. Demuth, *J. Chem. Phys.*, 1982, **76**, 6318.

125. C. W. Lim, J. M. Soon, N. L. Ma, W. Chen and K. P. Loh, *Surf. Sci.*, 2005, **575**, 51.

126. B. Sheu and D. R. Strongin, *J. Catal.*, 1995, **154**, 379.

127. S. Chaturvedi and D. R. Strongin, *J. Phys. Chem. B*, 1998, **102**, 2970.

128. B. A. Sexton, *Surf. Sci.*, 1979, **88**, 299.

129. N. F. Brown and M. A. Barteau, *J. Phys. Chem.*, 1996, **100**, 2269.

130. C. M. Whelan, F. Cecchet, R. Baxter, F. Zerbetto, G. Clarkson, D. Leigh and P. Rudolf, *J. Phys. Chem. B*, 2002, **106**, 8739.

131. C. M. Whelan, F. Cecchet, G. Clarkson, D. Leigh, R. Caudano and P. Rudolf, *Surf. Sci.*, 2001, **474**, 71.

132. J. E. Soto, Y. G. Kim, X. Chen, Y. S. Park and M. P. Soriaga, *J. Electroanal. Chem.*, 2001, **500**, 374.

133. M. P. Soriaga and A. T. Hubbard, *J. Am. Chem. Soc.*, 1982, **104**, 2735.

134. M. P. Soriaga, E. Binamira-Soriaga, A. T. Hubbard, J. B. Benziger and K. W. P. Pang, *Inorg. Chem.*, 1985, **24**, 65.

135. M. P. Soriaga, *Chem. Rev.*, 1990, **90**, 771.

136. F. Lu, G. N. Salaita, L. Laguren-Davidson, D. A. Stern, E. Wellner, D. G. Frank, N. Batina, D. C. Zapien, N. Walton and A. T. Hubbard, *Langmuir*, 1988, **4**, 637.

137. G. Salaita, L. Laguren-Davidson, F. Lu, N. Walton, E. Wellner, D. A. Stern, N. Batina, D. Frank, C. Lin and A. T. Hubbard, *J. Electroanal. Chem.*, 1988, **245**, 253.

138. J. E. Soto, Y. -G. Kim and M. P. Soriaga, *Electrochem. Commun.*, 1999, **1**, 135.

139. Y. -G. Kim, J. E. Soto, X. Chen, Y. -S. Park and M. P. Soriaga, *J. Electroanal. Chem.*, 2003, **554**, 167.

140. Y. -G. Kim and M. P. Soriaga, *Phys. Chem. Chem. Phys.*, 2001, **3**, 3303.

141. X. Chen, J. Sanabria-Chinchilla and M. P. Soriaga, *Electroanalysis*, 2005, **1**, 2121.

142. J. Breitbach, D. Franke, G. Hamm, C. Becker and K. Wandelt, *Surf. Sci.*, 2002, **507**, 18.

143. I. Jungwirthova and L. L. Kesmodel, *Surf. Sci.*, 2000, **470**, L39.

144. L. Bugyi, A. Oszko and F. Solymosi, *Surf. Sci.*, 2003, **539**, 1.

145. J. Eng, B. Bent, B. Fruhberger and J. G. Chen, *J. Phys. Chem. B*, 1997, **101**, 4044.

146. H. G. Huang, J. Y. Huang, Y. S. Ning and G. Q. Xu, *J. Chem. Phys.*, 2004, **121**, 4820.

147. M. Allan, *Chem. Phys.*, 1983, **81**, 235.

148. F. R. Yubero, J. P. Espinos, J. Cotrino and A. R. Gonzalez-Elipe, *Appl. Phys. Lett.*, 2005, **87**, 084101.

149. A. M. Botelho do Rego, O. Pellegrino, J. G. Martinho and J. Lopes da Silva, *Surf. Sci.*, 2001, **482**, 1228.

150. T. R. Bryden and J. Simon, *Langmuir*, 2001, **17**, 5850.

151. R. Becker, M. R. Ashton, T. S. Jones, N. V. Richardson and H. Sotobayashi, *J. Phys.: Condens. Matter*, 1991, **3**, S29.

152. W. P. McKenna and G. Apai, *J. Phys. Chem.*, 1992, **96**, 5902.

153. P. S. Dannetun and M. Rei Vilar, *Thin Solid Films*, 1996, **286**, 321.

154. N. J. Dinardo and T. C. Clarke, *Chem. Phys. Lett.*, 1985, **121**, 239.

155. J. -J. Pireaux, C. Gregoire, P. A. Thiry, R. Caudano and T. C. Clarke, *J. Chem. Phys.*, 1988, **88**, 3353.

156. A. Ulman, 'An Introduction to Ultrathin Organic Films: From Langmuir-Blodgett to Self-Assembly', Academic Press, New York, 1991.

157. A. Kudelski, *Vib. Spectrosc.*, 2005, **39**, 200.

158. H. S. Kato, J. Noh, M. Hara and M. Kawai, *J. Phys. Chem. B*, 2002, **106**, 9655.

159. J. Noh, H. S. Kato, M. Kawai and M. Hara, *J. Phys. Chem. B*, 2006, **110**, 2793.

160. A. S. Duwez, L. M. Yu, J. Riga, J. Delhalle and J. -J. Pireaux, *J. Phys. Chem. B*, 2000, **104**, 8830.

161. A. S. Duwez, L. M. Yu, J. Riga, J. -J. Pireaux and J. Delhalle, *Thin Solid Films*, 1998, **327**, 156.

162. A. S. Duwez, L. M. Yu, J. Riga, J. Delhalle and J. -J. Pireaux, *Langmuir*, 2000, **16**, 6569.

163. J. Noh, H. S. Kato, M. Kawai and M. Hara, *J. Phys. Chem. B*, 2002, **106**, 13268.

164. J. Gui, D. A. Stern, D. Frank, F. Lu, D. Zapien and A. T. Hubbard, *Langmuir*, 1991, **7**, 955.

165. B. G. Bravo, T. Mebrahtu and M. P. Soriaga, *Langmuir*, 1987, **3**, 595.